Robotica (2015) volume 33, pp. 1671–1685. © Cambridge University Press 2014
doi:10.1017/S0263574714000915

Influence of backlash in gear reducer on dynamic of single-link manipulator arm

Jian-Wei Lu†,*, Xiao-Ming Sun†,
Alexander F. Vakakis‡ and Lawrence A. Bergman§

†*School of Mechanical and Automotive Engineering, Hefei University of Technology, 230009 Hefei, Anhui, P. R. China*
‡*Department of Mechanical Science and Engineering, University of Illinois at Urbana-Champaign, Urbana 61801, USA*
§*Department of Aerospace Engineering, University of Illinois at Urbana-Champaign, Urbana 61801, USA*

(Accepted March 12, 2014. First published online: April 29, 2014)

SUMMARY
The dynamic modeling of a flexible single-link manipulator arm with consideration of backlash in the planetary gear reducer at the joint is presented, and the influence of backlash on the dynamic response of the system is evaluated. A 2K-H planetary gear reducer with backlash was employed as an example to discuss the dynamic modeling of the sub-model of the planetary gear reducer, and the sub-model of the planetary gear reducer was established based on the lumped mass method. The flexible manipulator was regarded as an Euler–Bernoulli beam, and the dynamic model of the flexible manipulator arm with backlash in the planetary gear reducer was determined from Lagrange's equations. Based on the this model, the influence of the backlash in the planetary gear reducer and excitation frequency on the dynamic response of the system were evaluated through simulation, and the results showed that the dynamic response of the system is sensitive to the backlash and the excitation frequency simultaneously, which provides a theoretical foundation for improvement of dynamic modeling and control of the flexible manipulator arm.

KEYWORDS: Backlash; Flexible manipulator arm; Planetary gear reducer; Dynamic behavior.

Nomenclature

$\theta_s, \theta_p, \theta_c$	Angular displacement of sun gear, planetary gear about its shaft, and carrier	r_s, r_p	Base circle radius of sun gear and planetary gear
I_s, I_p, I_c	Inertia moment of sun gear, planetary gear about its shaft, and carrier	r_c	Radius of carrier
b_{sp}, b_{pr}	Half of the backlash between sun gear and planetary gear, and that between planetary gear and ring gear	x_s, x_p, x_c	Equalized linear displacement of sun gear, planetary gear, and carrier
x_{sp}, x_{pr}	Relative displacement along the meshing line between sun gear and planetary gear, and that between planetary gear and ring gear	α	Pressure angle of the gear

* Corresponding author. E-mail: jwlu75@163.com

F_{ksp}, F_{csp}	Meshing spring force and damping force between sun gear and planetary gear	k_{sp}, c_{sp}	Meshing stiffness and meshing damping coefficient between sun gear and planetary gear
F_{kpr}, F_{cpr}	Meshing spring force and damping force planetary gear and ring gear	k_{pr}, c_{pr}	Meshing stiffness and meshing damping coefficient between planetary gear and ring gear
m_p	Mass of the planetary gear	I_{arm}	Inertia moment of manipulator arm connected to carrier
X_{sp}, X_{pr}, X_c	Dimensionless parameters corresponding to x_{sp},x_{pr},x_c	A, ρ, EI	Section area, linear density, and bending rigidity of manipulator arm
L	Length of manipulator arm	$\Delta\theta$	Angular displacement error of rigid manipulator arm due to backlash of gear reducer
f_{la}	Positioning error at the end of the flexible manipulator arm	dr	Flexible deformation of the manipulator arm

1. Introduction

Manipulator arms have many advantages, including reducing human labor, avoiding dangerous working environments, and precision operation. Today, more and more manipulator arms are applied in industrial settings to supplement or replace human operators. At the same time, greater performance requirements of the manipulator arm are desired, including higher speeds, greater load/weight ratios, and higher positioning precision. The flexible manipulator arm is regarded as an efficient choice to achieve greater load/weight ratios, but the flexibility of the arm under high-speed working conditions often leads to severe vibration of the arm, resulting in deterioration of the positioning precision. As a result, research on vibration control of flexible manipulator arms and improvement of their positioning precision has received much attention in recent decades.[1–5] Dynamic modeling of the manipulator is the basis for effective vibration control, and much effort has been devoted to that end.

For example, Mehrdad[6] proposed a redundant Lagrangian/finite element approach to model the dynamics of lightweight spatial manipulators with both flexible links and joints; Albedoor[7] presented a linearized dynamic model for multi-link planar flexible manipulators which can include an arbitrary number of flexible links; Subudhi[8] presented a dynamic modeling technique for a manipulator with multiple flexible links and flexible joints, based on a combined Euler–Lagrange formulation and assumed modes method; Green[9] discussed the dynamic modeling of a manipulator with flexible links, where nonlinear rigid-link dynamics are coupled with dominant assumed modes for cantilever and pinned-pinned beams; Fotouhi[10] studied the dynamic modeling and analysis of very flexible beams with large deflections using a finite element approach; Vakil[11] provided closed-form dynamic equations of planar flexible-link manipulators (FLMs) with revolute joints and constant cross-sections based on Lagrange's equations and the assumed mode shape method, which can be used for the model-based end-effecter control and the vibration suppression of planar FLMs; Kalyoncu[12] investigated the mathematical modeling and dynamic response of a flexible robot manipulator with rotating-prismatic joint; Zhou[13] provided a method to determine the variable flexible-joint parameters which are dependent on configurations for a PRS (prismatic pairs-revolute joints-spherical joints) parallel robot, which is applicable to flexible multi-body systems with variable configurations; Yesiloglu[14] presented the dynamic model of a co-operating under-actuated flexible manipulator with active joints; Rognant[15] provided a systematic procedure for the elasto-dynamic modeling of an industrial robot, in which flexible links and joints were considered; Korayem[16] presented the kinematics and dynamics equations of a manipulator with flexible joints, and a computational technique for obtaining maximum load carrying capacity of robotic manipulators with joint elasticity was discussed; Chen[17] proposed the rigid–flexible coupled dynamics model of a 4-UPS-RPS (universal joints-prismatic pairs-spherical joints-revolute joints-prismatic pairs-spherical joints) parallel robot, in which, the driving limbs and spherical joints were treated as flexible bodies, while the moving platform, stationary platform, and other joints of parallel robot were treated as rigid bodies; Zarafshan[18] developed a compact rigid–flexible interactive dynamics model of multi-body systems composed of rigid and flexible

https://doi.org/10.1017/S0263574714000915 Published online by Cambridge University Press

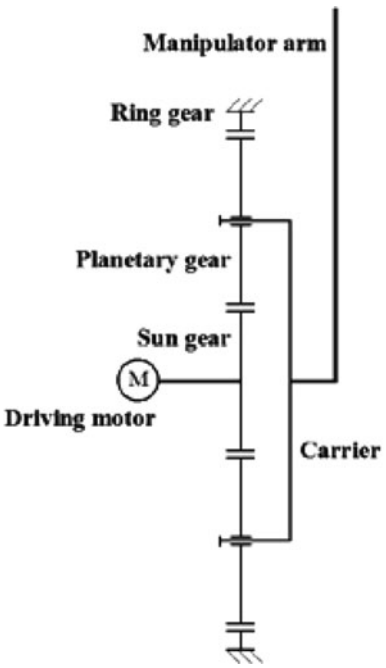

Fig. 1. Diagram of manipulator with planetary gear reducer at the joint.

elements, and as a result, less computation cost on the model was obtained; Vakil[19] proposed a new method for dynamic modeling of flexible-link flexible-joint manipulator; Pratiher[20] investigated the nonlinear dynamic modeling and analysis of a Cartesian manipulator carrying an end effector which was placed at different intermediate positions on the span with a single mode approach.

While these works provide a good basis for improvement of the dynamic modeling of the manipulator with flexible links and joints, it should be noted that they are all based on the assumption of no clearance in the mechanism; clearly, though, backlash in the planetary gear reducer is generally inevitable and can greatly influence the dynamic response of the gear system and the dynamic response of the flexible manipulator arm connected to the gear reducer. Therefore, it is necessary to analyze the effect of backlash on the dynamic response of the flexible manipulator arm, in order to improve the performance of the manipulator arm.

In this paper, the dynamic modeling of a planetary gear reducer with backlash was studied using the lumped mass method, and a dynamic model of a single-link manipulator arm with backlash in the planetary gear reducer was presented. Based on the model, the influence of backlash on the dynamic response of the system was evaluated, which will provide basis for further improvement of dynamic modeling and positioning control of flexible manipulator arms.

2. Sub-Model of the Planetary Gear Reducer with Backlash

The diagram of the manipulator with planetary gear reducer at the joint is shown in Fig. 1, in which, the driving motor is connected to the sun gear and the manipulator arm is connected to the carrier.

Without loss of generality, a 2K-H-type planetary gear mechanism was taken as an example for dynamic modeling of the planetary gear reducer. The diagram of the planetary gear reducer with backlash is shown in Fig. 2, in which, there is backlash between the sun gear and planetary gear and between the planetary gear and gear ring.

The angular displacement of the component can be equalized to linear displacement along the meshing line, in which, the equalized linear displacement of sun gear is given by

$$x_s = r_s \theta_s. \tag{1}$$

https://doi.org/10.1017/S0263574714000915 Published online by Cambridge University Press

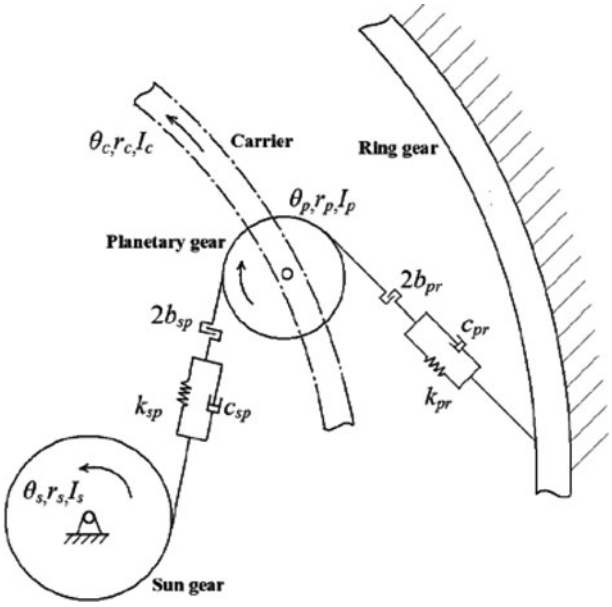

Fig. 2. Diagram of planetary gear reducer with backlash.

The equalized linear displacement of planetary gear is given by

$$x_p = r_p \theta_p. \tag{2}$$

For the carrier, its radius r_c plays the similar role as the reference circle of gears, therefore, the equivalent base radius of carrier is written as $r_c \cos \alpha$, and the equivalent linear displacement along the meshing line for angular displacement of carrier should be given by

$$x_c = r_c \theta_c \cos \alpha. \tag{3}$$

The relative displacement along the meshing line between the sun gear and the planetary gear can be given as

$$x_{sp} = x_s - x_p - x_c \tag{4}$$

The relative displacement along the meshing line between the planetary gear and the ring gear can be given as

$$x_{pr} = x_p - x_c. \tag{5}$$

The meshing spring force F_{ksp} and damping force F_{csp} between sun gear and planetary gear are given by[22]

$$\begin{cases} F_{ksp} = k_{sp} f_k(x_{sp}, b_{sp}) \\ F_{csp} = c_{sp} f_c(x_{sp}, b_{sp}) \end{cases}, \tag{6}$$

in which,

$$f_k(p, b) = \begin{cases} p - b & p > b \\ 0 & -b \le p \le b \\ p + b & p < -b \end{cases}, \tag{7}$$

$$f_c(p, b) = \begin{cases} \dot{p} & |p| > b \\ 0 & |p| \le b \end{cases}. \tag{8}$$

https://doi.org/10.1017/S0263574714000915 Published online by Cambridge University Press

The meshing spring force F_{kpr} and damping force F_{cpr} between planetary gear and ring gear are given by

$$\begin{cases} F_{kpr} = k_{pr} f_k(x_{pr}, b_{pr}) \\ F_{cpr} = c_{pr} f_c(x_{pr}, b_{pr}) \end{cases}. \tag{9}$$

The equilibrium equations of the system can be written as

$$\begin{cases} I_s \ddot{\theta}_s + 3(F_{csp} + F_{ksp} + F_{cpr} + F_{kpr}) r_s = T_M \\ I_p \ddot{\theta}_p - (F_{csp} + F_{ksp} - F_{cpr} - F_{kpr}) r_p = 0 \\ (I_c + I_{arm} + 3m_p r_c^2)\ddot{\theta}_s - 3(F_{csp} + F_{ksp} - F_{cpr} - F_{kpr}) r_c \cos\alpha = 0 \end{cases}, \tag{10}$$

in which, the driving torque of the driving motor is

$$T_M = a_m - b_m \dot{\theta}_s + F_w \sin \omega t, \tag{11}$$

where a_m and b_m are constants provided by the motor manufacture, and $F_w \sin \omega t$ is the output torque fluctuation of the motor.

Then Eq. (10) can be rewritten as

$$\begin{cases} \ddot{x}_{sp} + \dfrac{1}{M_{sp}} F_{csp} + \dfrac{B_m}{M_s} \dot{x}_{sp} + \dfrac{B}{M_{sp}} F_{cpr} + \dfrac{B_m}{M_s} \dot{x}_c + \dfrac{1}{M_{sp}} F_{ksp} + \dfrac{B}{M_{sp}} F_{kpr} = \dfrac{A_m}{M_s} \\ \ddot{x}_{pr} + \dfrac{D}{M_{pr}} F_{csp} + \dfrac{1}{M_{pr}} F_{cpr} + \dfrac{D}{M_{pr}} F_{ksp} + \dfrac{1}{M_{pr}} F_{kpr} = 0 \\ \ddot{x}_c - \dfrac{3}{M_c'} F_{csp} - \dfrac{3}{M_c'} F_{cpr} - \dfrac{3}{M_c'} F_{ksp} - \dfrac{3}{M_c'} F_{kpr} = 0 \end{cases}, \tag{12}$$

in which,

$$\begin{aligned} M_s &= \frac{I_s}{r_s^2}, \quad M_p = \frac{I_p}{r_p^2}, \quad A_m = \frac{a_m}{r_s}, \quad B_m = \frac{b_m}{r_s^2}, \\ M_c &= \frac{I_c}{r_c^2 \cos^2\alpha}, \quad M_c' = M_c + \frac{3m_p}{\cos^2\alpha} + \frac{I_{arm}}{r_c^2 \cos^2\alpha}, \\ M_{sp} &= \frac{M_s M_p M_c'}{3M_p M_c' + M_s M_c' + 3M_s M_p}, \quad M_{pr} = \frac{M_p M_c'}{3M_p + M_c'}, \\ D &= \frac{3M_p - M_c'}{3M_p + M_c'}, \quad B = \frac{3M_s M_p - M_s M_c'}{3M_p M_c' + M_s M_c' + 3M_s M_p}. \end{aligned}$$

The nominal time scale ω_n and nominal displacement scale b_c are introduced to make Eq. (12) dimensionless.

The dimensionless time parameter is $\tau = \omega_n t$, and

$$X = b_c x, \tag{13}$$

$$\dot{X} = b_c \omega_n \dot{x}, \tag{14}$$

$$\ddot{X} = b_c \omega_n^2 \ddot{x}. \tag{15}$$

https://doi.org/10.1017/S0263574714000915 Published online by Cambridge University Press

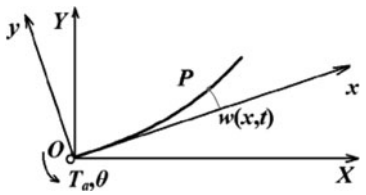

Fig. 3. Diagram of flexible manipulator arm.

Therefore, the dimensionless equations of the system are given by

$$\begin{cases} \ddot{X}_{sp} + \dfrac{1}{M_{sp}\omega_n} F_{csp} + \dfrac{B_m}{M_s\omega_n}\dot{X}_{sp} + \dfrac{B_m}{M_s\omega_n}\dot{X}_{pr} + \dfrac{2B_m}{M_s\omega_n}\dot{X}_c + f_k(X_{sp}) + \dfrac{B}{M_{sp}\omega_n^2} F_{kpr} = \dfrac{A_m}{M_{sp}b_c\omega_n^2} \\ \ddot{X}_{pr} + \dfrac{D}{M_{sp}\omega_n} F_{csp} + \dfrac{1}{M_{pr}\omega_n} F_{cpr} + \dfrac{DM_{sp}}{M_{pr}} f_k(X_{sp}) + \dfrac{1}{M_{pr}\omega_n^2} F_{kpr} = 0 \\ \ddot{X}_c - \dfrac{3}{M_c'\omega_n} F_{csp} - \dfrac{3}{M_c'\omega_n} F_{cpr} - \dfrac{3M_{sp}}{M_c'} f_k(X_{sp}) - \dfrac{3}{M_c'\omega_n^2} F_{kpr} = 0 \end{cases} . \tag{16}$$

3. Dynamic Model of Flexible Manipulator Arm with Backlash in Planetary Gear Reducer

The diagram of a single-link flexible manipulator arm is shown as Fig. 3. It is assumed that its shearing deformation is negligible compared with its bending deformation, and it can be regarded as an Euler–Bernoulli beam. The displacement of the an arbitrary point P on the arm is given by $w(x,t)$.

The flexible manipulator arm can be regarded as a beam with one end fixed and the other end free; therefore, the mode shape associated with its rth mode is given by

$$\varphi_r = (\sin\beta_r x - sh\beta_r x) + \xi_r(\cos\beta_r x - ch\beta_r x), \tag{17}$$

in which, β_r and ξ_r can be given by

$$\beta_r = \frac{\pi}{l}\left(r - \frac{1}{2}\right), \tag{18}$$

$$\xi_r = \frac{\cos\beta_r l + ch\beta_r l}{\sin\beta_r l + sh\beta_r l}. \tag{19}$$

The mode coordinate of ith mode is $q_i(t)$, and the displacement of point P can be written as

$$w(x,t) = \sum_{i=1}^{S} \varphi_i(x) q_i(t), \tag{20}$$

in which, S is the modal truncation order.

The kinetic energy and deformation potential energy of the manipulator arm is given by

$$\begin{cases} T = \dfrac{1}{2}\displaystyle\int_0^l \rho A \left[\frac{\partial w(x,t)}{\partial t}\right]^2 dx \\ V = \dfrac{1}{2}\displaystyle\int_0^l EI \left[\frac{\partial^2 w(x,t)}{\partial x^2}\right]^2 dx \end{cases} . \tag{21}$$

Based on the work presented above, the equations of motion (EOM) of the system can be obtained by Lagrange's equations, in which the modal truncation order S is determined by convergence considerations. The dynamic response of the deformation at the end of the manipulator arm without backlash in the gear reducer for different modal truncation orders is calculated to determine when

https://doi.org/10.1017/S0263574714000915 Published online by Cambridge University Press

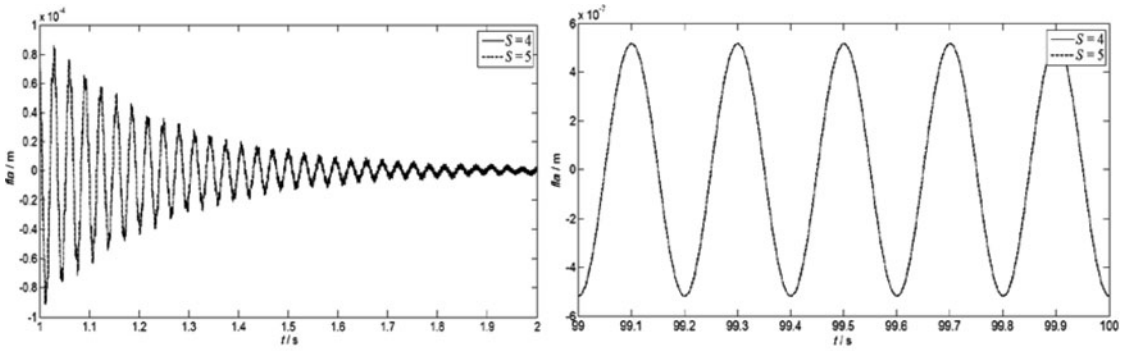

Fig. 4. Comparison of the results with different modal truncation order.

convergence is achieved. The results with modal truncation order $S = 4$ and $S = 5$ are shown in Fig. 4. It can be seen that for the difference in the result between modal truncation orders $S = 4$ and $S = 5$ is small, which implies that the former is precise enough.

With modal truncation order $S = 4$, the EOMs of the system can be written as

$$\begin{cases} \ddot{X}_{sp} = \dfrac{a_{11}}{b_0\omega_n^2} + \dfrac{a_{12}}{\omega_n}\dot{X}_{sp} + \dfrac{a_{12}}{\omega_n}\dot{X}_{pr} + \dfrac{a_{13}}{\omega_n}\dot{X}_c + \dfrac{a_{14}}{\omega_n^2}f_k(X_{sp}) + \dfrac{a_{15}}{\omega_n}f_c(X_{sp}) + \dfrac{a_{16}}{\omega_n^2}f_k(X_{pr}) \\ \quad + \dfrac{a_{17}}{\omega_n}f_c(X_{pr}) + \dfrac{a_{18}}{\omega_n^2}\bar{q}_1 + \dfrac{a_{19}}{\omega_n^2}\bar{q}_2 + \dfrac{a_{110}}{\omega_n^2}\bar{q}_3 + \dfrac{a_{111}}{\omega_n^2}\bar{q}_4 \\ \ddot{X}_{pr} = \dfrac{a_{21}}{\omega_n^2}f_k(X_{sp}) + \dfrac{a_{22}}{\omega_n}f_c(X_{sp}) + \dfrac{a_{23}}{\omega_n^2}f_k(X_{pr}) + \dfrac{a_{24}}{\omega_n}f_c(X_{pr}) + \dfrac{a_{18}}{\omega_n^2}\bar{q}_1 + \dfrac{a_{19}}{\omega_n^2}\bar{q}_2 + \dfrac{a_{110}}{\omega_n^2}\bar{q}_3 + \dfrac{a_{111}}{\omega_n^2}\bar{q}_4 \\ a_{30}\ddot{X}_c = \dfrac{a_{31}}{\omega_n^2}\bar{q}_1 + \dfrac{a_{32}}{\omega_n^2}\bar{q}_2 + \dfrac{a_{33}}{\omega_n^2}\bar{q}_3 + \dfrac{a_{34}}{\omega_n^2}\bar{q}_4 + \dfrac{a_{35}}{\omega_n^2}f_k(X_{sp}) + \dfrac{a_{36}}{\omega_n}f_c(X_{sp}) + \dfrac{a_{37}}{\omega_n^2}f_k(X_{pr}) + \dfrac{a_{38}}{\omega_n}f_c(X_{pr}) \\ a_{40}\ddot{\bar{q}}_1 = \dfrac{a_{41}}{\omega_n^2}\bar{q}_1 + \dfrac{a_{42}}{\omega_n^2}\bar{q}_2 + \dfrac{a_{43}}{\omega_n^2}\bar{q}_3 + \dfrac{a_{44}}{\omega_n^2}\bar{q}_4 + \dfrac{a_{45}}{\omega_n^2}f_k(X_{sp}) + \dfrac{a_{46}}{\omega_n}f_c(X_{sp}) + \dfrac{a_{47}}{\omega_n^2}f_k(X_{pr}) + \dfrac{a_{48}}{\omega_n}f_c(X_{pr}) \\ a_{50}\ddot{\bar{q}}_2 = \dfrac{a_{51}}{\omega_n^2}\bar{q}_1 + \dfrac{a_{52}}{\omega_n^2}\bar{q}_2 + \dfrac{a_{53}}{\omega_n^2}\bar{q}_3 + \dfrac{a_{54}}{\omega_n^2}\bar{q}_4 + \dfrac{a_{55}}{\omega_n^2}f_k(X_{sp}) + \dfrac{a_{56}}{\omega_n}f_c(X_{sp}) + \dfrac{a_{57}}{\omega_n^2}f_k(X_{pr}) + \dfrac{a_{58}}{\omega_n}f_c(X_{pr}) \\ a_{60}\ddot{\bar{q}}_2 = \dfrac{a_{61}}{\omega_n^2}\bar{q}_1 + \dfrac{a_{62}}{\omega_n^2}\bar{q}_2 + \dfrac{a_{63}}{\omega_n^2}\bar{q}_3 + \dfrac{a_{64}}{\omega_n^2}\bar{q}_4 + \dfrac{a_{65}}{\omega_n^2}f_k(X_{sp}) + \dfrac{a_{66}}{\omega_n}f_c(X_{sp}) + \dfrac{a_{67}}{\omega_n^2}f_k(X_{pr}) + \dfrac{a_{68}}{\omega_n}f_c(X_{pr}) \\ a_{70}\ddot{\bar{q}}_2 = \dfrac{a_{71}}{\omega_n^2}\bar{q}_1 + \dfrac{a_{72}}{\omega_n^2}\bar{q}_2 + \dfrac{a_{73}}{\omega_n^2}\bar{q}_3 + \dfrac{a_{74}}{\omega_n^2}\bar{q}_4 + \dfrac{a_{75}}{\omega_n^2}f_k(X_{sp}) + \dfrac{a_{76}}{\omega_n}f_c(X_{sp}) + \dfrac{a_{77}}{\omega_n^2}f_k(X_{pr}) + \dfrac{a_{78}}{\omega_n}f_c(X_{pr}) \end{cases}, \tag{22}$$

in which,

$$\bar{q}_i = b_c q_i, \ddot{\bar{q}}_i = b_c\omega_n^2 q_i, \quad a_{01} = \frac{I_c + 3m_p r_c^2 + I_{arm}}{r_c\cos\alpha}, \quad a_{0(i+1)} = \frac{\rho A\int_0^l x\varphi_i dx}{r_c\cos\alpha},$$

$$a_{11} = \frac{A_m}{M_s}, \quad a_{12} = -\frac{B_m}{M_s}, \quad a_{13} = 2a_{12}, \quad a_{14} = -\left(\frac{3}{M_s} + \frac{1}{M_p} + \frac{a_{36}}{a_{30}}\right)k_{sp}, \quad a_{15} = \frac{a_{14}}{k_{sp}}c_{sp},$$

$$a_{16} = -\left(\frac{3}{M_s} - \frac{1}{M_p} + \frac{a_{36}}{a_{30}}\right)k_{pr}, \quad a_{17} = \frac{a_{16}}{k_{pr}}c_{pr}, \quad a_{18} = -\frac{a_{31}}{a_{30}}, \quad a_{19} = -\frac{a_{32}}{a_{30}},$$

$$a_{110} = -\frac{a_{33}}{a_{30}}, \quad a_{111} = -\frac{a_{34}}{a_{30}}, \quad a_{21} = \left(\frac{1}{M_p} - \frac{a_{36}}{a_{30}}\right)k_{sp}, \quad a_{22} = \frac{a_{21}}{k_{sp}}c_{sp},$$

$$a_{23} = -\left(\frac{1}{M_p} + \frac{a_{36}}{a_{30}}\right)k_{pr}, \quad a_{24} = \frac{a_{23}}{k_{pr}}c_{pr}, \quad a_{30} = a_{01} - \sum_{i=1}^{4}\frac{\rho A\int_0^l x\varphi_i dx}{\rho A\int_0^l \varphi_i^2 dx}a_{0(i+1)},$$

$$a_{3i} = \frac{\rho A\int_0^l x\varphi_i dx\int_0^l EI\left(\frac{d^2\varphi_i}{dx^2}\right)^2 dx}{\rho A\int_0^l \varphi_i^2 dx} \qquad (i = 1, 2, 3, 4),$$

https://doi.org/10.1017/S0263574714000915 Published online by Cambridge University Press

Table I. Parameters of the system used for numerical analysis.

Parameter	Value/unit	Parameter	Value/unit
z_s	27	ρ	$7900/Kg/m^3$
z_p	36	A	$1e-4/m^2$
z_r	99	l	0.5/m
m	3.0/mm	m_p	0.66/Kg
α	24.6/°	I_s/r_s^2	0.39/Kg
k_{sp}	1e8/ N/m	I_p/r_p^2	0.61/Kg
k_{pr}	1e8/N/m	I_c/r_c^2	6.29/Kg
E	2e11/Pa	I_{arm}	$0.033/Kg/m^2$

$$a_{35} = 3r_c \cos\alpha k_{sp}, \quad a_{36} = 3r_c \cos\alpha c_{sp}, \quad a_{37} = 3r_c \cos\alpha k_{pr}, \quad a_{38} = 3r_c \cos\alpha c_{pr},$$

$$a_{40} = a_{30}\rho A \int_0^l \varphi_1^2 dx, \quad a_{41} = -a_{30} \int_0^l EI \left(\frac{d^2\varphi_1}{dx^2}\right)^2 dx - a_{02}a_{31},$$

$$a_{4j} = -a_{02}a_{3j} \quad (j = 2, 3, \ldots, 8),$$

$$a_{50} = a_{30}\rho A \int_0^l \varphi_2^2 dx, \quad a_{52} = -a_{30} \int_0^l EI \left(\frac{d^2\varphi_2}{dx^2}\right)^2 dx - a_{03}a_{32},$$

$$a_{5k} = -a_{03}a_{3k} \quad (k = 1, 3, \ldots, 8),$$

$$a_{60} = a_{30}\rho A \int_0^l \varphi_3^2 dx, \quad a_{63} = -a_{30} \int_0^l EI \left(\frac{d^2\varphi_3}{dx^2}\right)^2 dx - a_{03}a_{33},$$

$$a_{6m} = -a_{04}a_{3m} \quad (m = 1, 2, 4, \ldots, 8),$$

$$a_{70} = a_{30}\rho A \int_0^l \varphi_4^2 dx, \quad a_{74} = -a_{30} \int_0^l EI \left(\frac{d^2\varphi_4}{dx^2}\right)^2 dx - a_{03}a_{34},$$

$$a_{7n} = -a_{05}a_{3n} \quad (n = 1, \ldots, 3, 5, \ldots, 8).$$

The transmission ratio from sun gear to carrier is marked as i_{sH}, and the angular displacement error of the rigid manipulator arm due to backlash of the gear reducer can be given by

$$\Delta\theta = \frac{1}{r_s i_{sH}}(x_{sp} + x_{pr}). \tag{23}$$

The positioning error at the end of the flexible manipulator arm includes two components: the transmission error due to the backlash of the gear reducer and the flexible deformation of the manipulator arm. It can be written as

$$f_{la} = l\Delta\theta + w(l,t) = \frac{l}{r_s i_{sH}}(x_{sp} + x_{pr}) + \sum_{i=1}^{4} \varphi_i(l) q_i(t). \tag{24}$$

4. Numerical Analysis

Based on the model presented above, the dynamic response of the flexible manipulator arm, considering backlash in the planetary gear reducer, is examined through numerical examples, and the influence of the backlash on the dynamic response of the system is evaluated, in which, Adams multi-step integral method is applied for the numerical analysis.[21] Here, it is assumed that there is uniform backlash in the gear pairs of the planetary gear reducer and the backlash between gear teeth is given by 2b, and that the manipulator is operated free of loading. The parameters used for the numerical analysis are listed as Table I.

https://doi.org/10.1017/S0263574714000915 Published online by Cambridge University Press

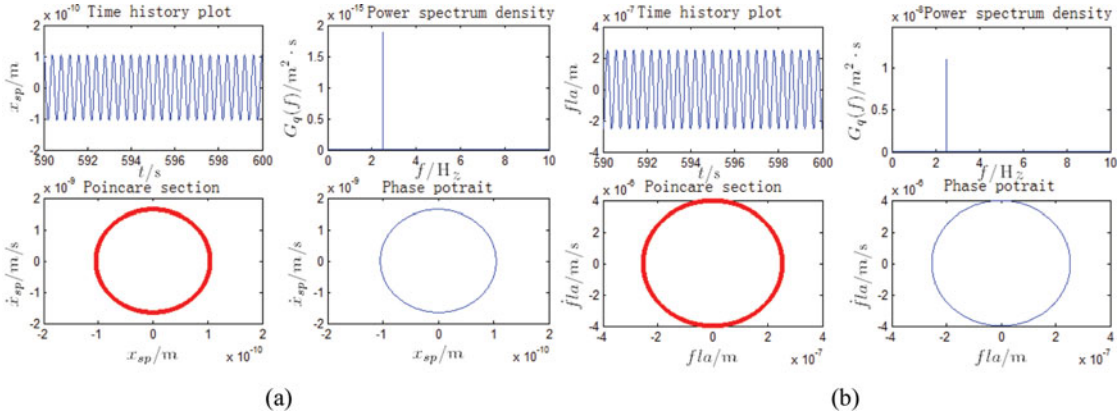

Fig. 5. Dynamic response of the system with flexible arm ($b = 0\ \mu$ m, $\omega = 5\pi$).

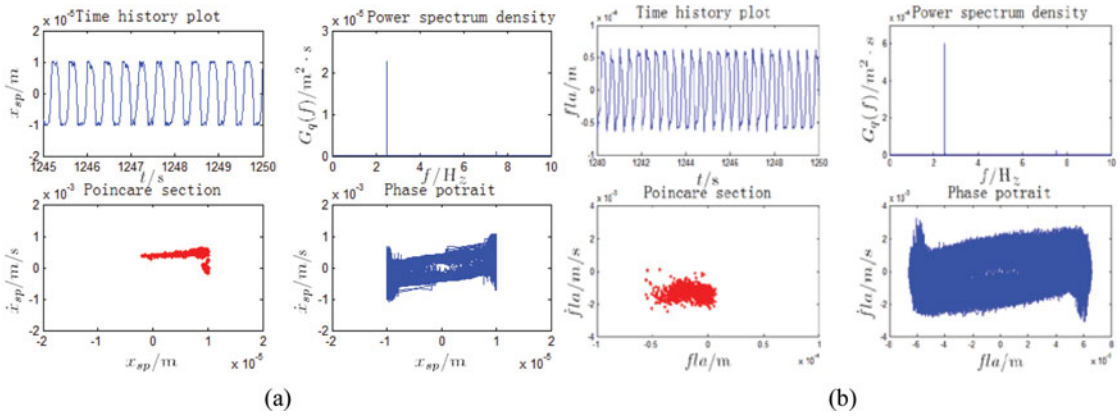

Fig. 6. Dynamic response of the system with flexible arm ($b = 10\ \mu$ m, $\omega = 5\pi$).

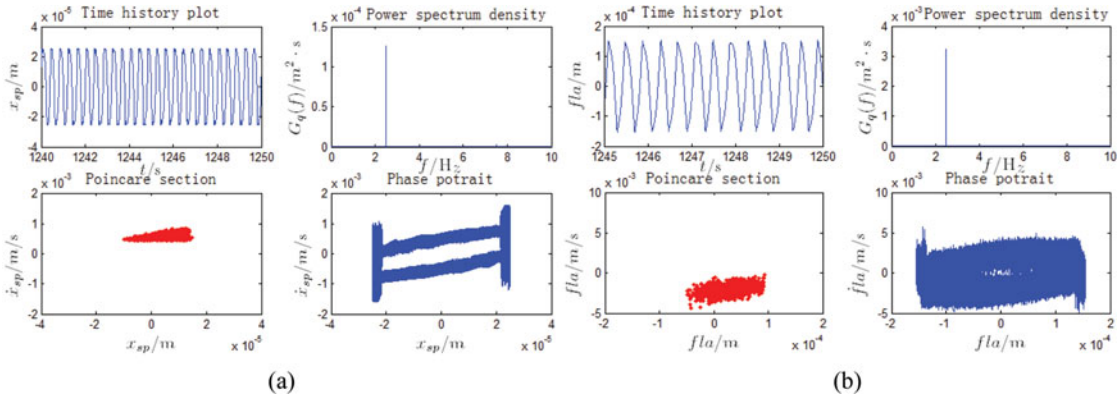

Fig. 7. Dynamic response of the system with flexible arm ($b = 25\ \mu$ m, $\omega = 5\pi$).

4.1. The influence of backlash on the dynamic behavior of the system

If the frequency of harmonic fluctuation of the output torque of the motor is $\omega = 5\pi$, the dynamic responses of the system with backlash given successively by $b = 0\ \mu$m, $10\ \mu$m, $25\ \mu$m, $50\ \mu$m, $100\ \mu$m are calculated. The transmission error between the sun gear and planetary gear x_{sp} and the positioning error at the end of the manipulator arm f_{la} are presented in order to evaluate the dynamic response of the gear reducer and the manipulator arm, and the results are shown as Figs. 5–9, in which (a) is the results of x_{sp} and (b) shows the results of f_{la}. And the figure of $Gq(f)$ shows the power spectrum density of displacement.

From these numerical results, it can be seen that backlash has a significant effect on the dynamic behavior of the system. The dynamic responses of the gear reducer and flexible manipulator arm experience variation

https://doi.org/10.1017/S0263574714000915 Published online by Cambridge University Press

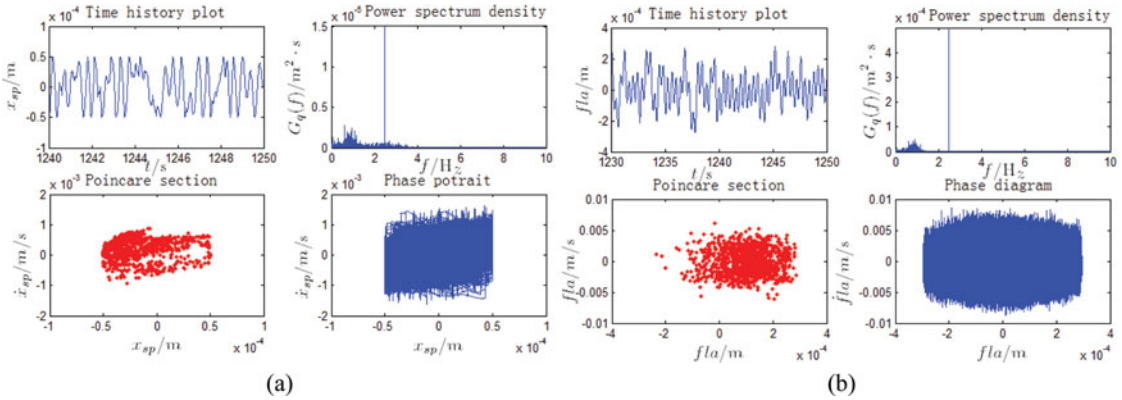

Fig. 8. Dynamic response of the system with flexible arm ($b = 50\ \mu$ m, $\omega = 5\pi$).

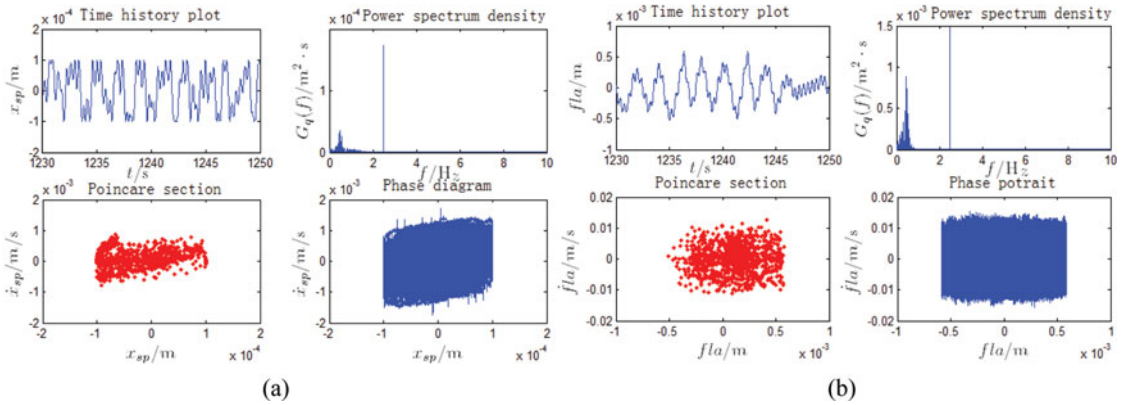

Fig. 9. Dynamic response of the system with flexible arm ($b = 100\ \mu$ m, $\omega = 5\pi$).

from quasi-period motion to chaos with increasing backlash, and the positioning error at the end of the flexible manipulator arm increases with the backlash.

As mentioned above, the positioning error at the end of the flexible manipulator arm is composed of two components: the transmission error due to the backlash of the gear reducer and the flexible deformation of the manipulator arm. The dominant component is the flexible deformation if the backlash is small, while the transmission error due to the backlash of the gear reducer gradually becomes the dominant component with increasing backlash. The flexible deformations of the manipulator arm dr as a function of backlash in the gear reducer are shown as Fig. 10, in which, (a), (b), (c), and (d) are the results with $b = 10\ \mu$m, 25 μm, 50 μm, 100 μm, respectively.

It can be seen that when the backlash is small, for example, $b = 10\ \mu$m, 25 μm, 50 μm, the dominant frequency of the flexible deformation of the manipulator arm dr is its 1st mode; while if the backlash increases to 100 μm, its dominant frequency becomes the 3rd mode, which results from the influence of the nonlinearity of the gear reducer.

4.2. The influence of excitation frequency on the dynamic behavior of the system

When the frequency of harmonic fluctuation of the output torque of the motor is $\omega = 10\pi$, the system responses for backlash $b = 0\ \mu$m, 10 μm, 25 μm, 50 μm, 100 μm are shown as Figs. 11–15, in which, (a) is the result for x_{sp} and (b) is the result for f_{la}.

Comparison of the results for $\omega = 5\pi$ and $\omega = 10\pi$ reveals that the dynamic behavior of the system is sensitive to clearance and excitation frequency simultaneously. When the excitation is $\omega = 5\pi$, the motion of the gear reducer is quasi-period with $b = 10\ \mu$m, 25 μm, while it becomes chaotic with $b = 50\ \mu$m, 100 μm. When the excitation is $\omega = 10\pi$, the motion of the gear reducer is quasi-period with $b = 10\ \mu$m, but chaotic with $b = 25\ \mu$m, 50 μm, 100 μm.

https://doi.org/10.1017/S0263574714000915 Published online by Cambridge University Press

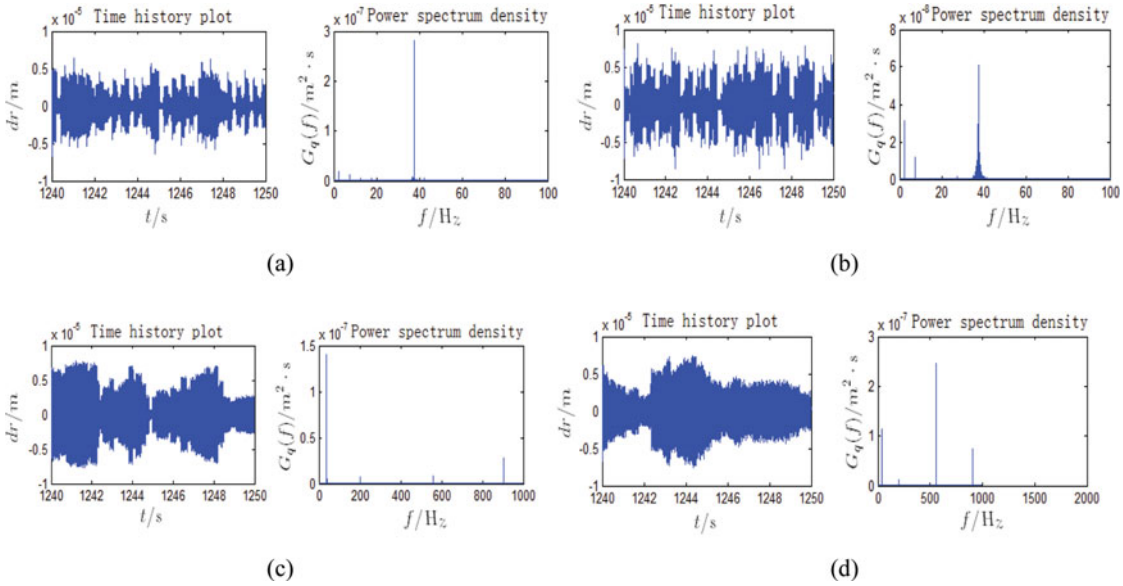

Fig. 10. Flexible deformation of the manipulator arm dr ($\omega = 5\pi$).

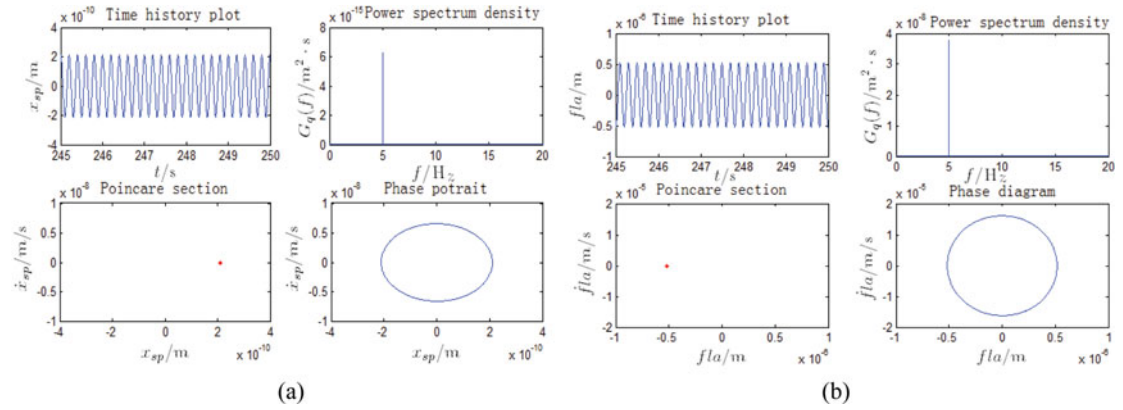

Fig. 11. Dynamic response of the system with flexible arm ($b = 0$ μm, $\omega = 10\pi$).

4.3. The influence of flexibility of the manipulator arm on the dynamic behavior of the gear reducer
If the manipulator arm is taken to be rigid, the transmission error between the sun gear and planetary gear x_{sp} for excitation frequency $\omega = 10\pi$, and backlash $b = 10$ μm, 25 μm, 50 μm, 100 μm is shown as Figs. 16–19. Comparing the results of the system with rigid arm flexible arm, it is found that the dynamic behavior of the gear reducer is significantly influenced by the flexibility. For example, if the backlash $b = 100$ μm, the response of the gear system with rigid arm is quasi-period motion, while the response of system with flexible manipulator arm with the same backlash is chaotic; this is likely the result of the interaction between the dynamic response of the flexible manipulator arm and gear reducer.

5. Conclusions

Backlash in the planetary gear reducer was taken into consideration in the modeling of a manipulator arm, and its influence on the dynamic response of the system was evaluated. A two-state model was used to describe the meshing forces at the gear pairs of the planetary gear reducer with backlash, and the sub-model of the planetary gear reducer was presented as a lumped mass method. The deformation of the manipulator arm was based on Euler–Bernoulli beam theory, and the dynamic model of the manipulator arm with planetary gear reducer was obtained. Numerical analysis based on the Adams multi-step integral method was carried out to evaluate the dynamic response of the system incorporating backlash in the planetary gear reducer, and the following conclusions were obtained:

https://doi.org/10.1017/S0263574714000915 Published online by Cambridge University Press

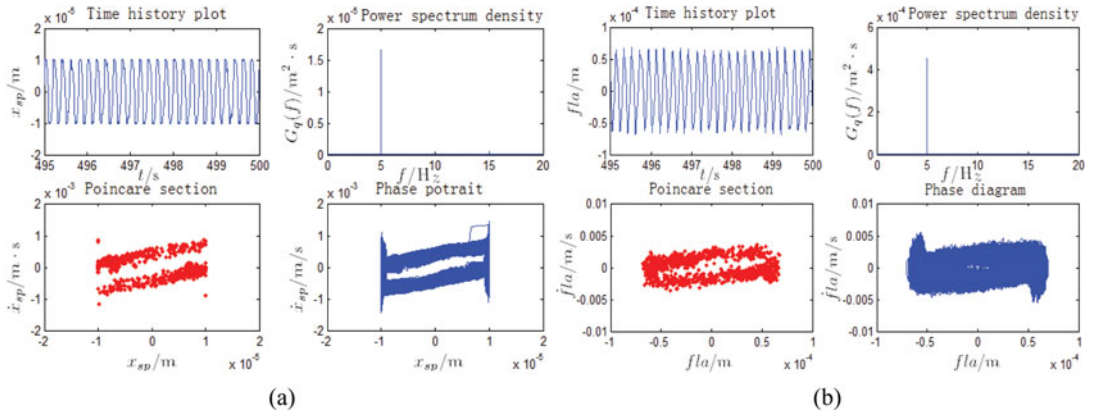

Fig. 12. Dynamic response of the system with flexible arm ($b = 10\ \mu$m, $\omega = 10\pi$).

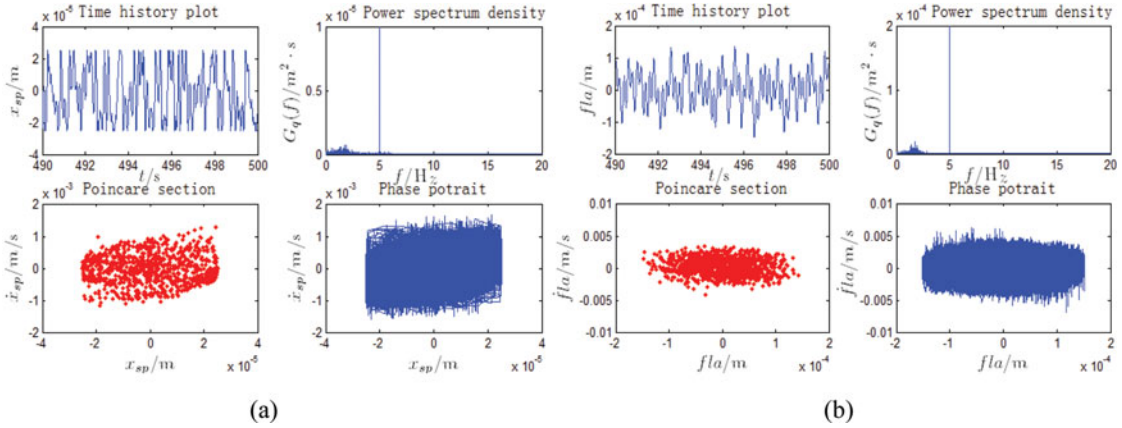

Fig. 13. Dynamic response of the system with flexible arm ($b = 25\ \mu$m, $\omega = 10\pi$).

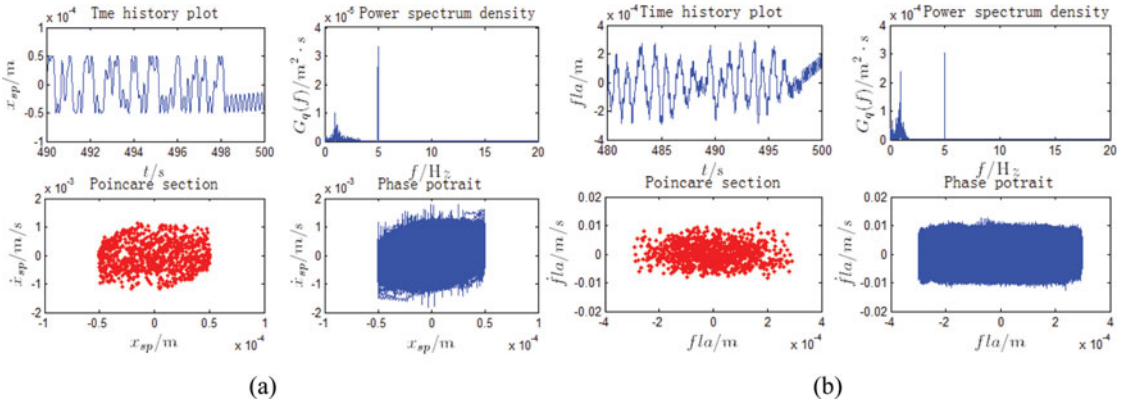

Fig. 14. Dynamic response of the system with flexible arm ($b = 50\ \mu$m, $\omega = 10\pi$).

(1) The backlash in the planetary gear reducer has a significant effect on the dynamic response of the system and contributes to the positioning precision of the manipulator arm. Therefore, it is necessary to take the backlash of the gear reducer into consideration in the dynamic modeling of the manipulator.
(2) The responses of the planetary gear reducer and flexible manipulator arm vary from quasi-period motion to chaos as the backlash increases. However, it should be noted that the dynamic behavior of the system is also sensitive to the excitation frequency; a change of excitation frequency can cause significant variation in their motions.

https://doi.org/10.1017/S0263574714000915 Published online by Cambridge University Press

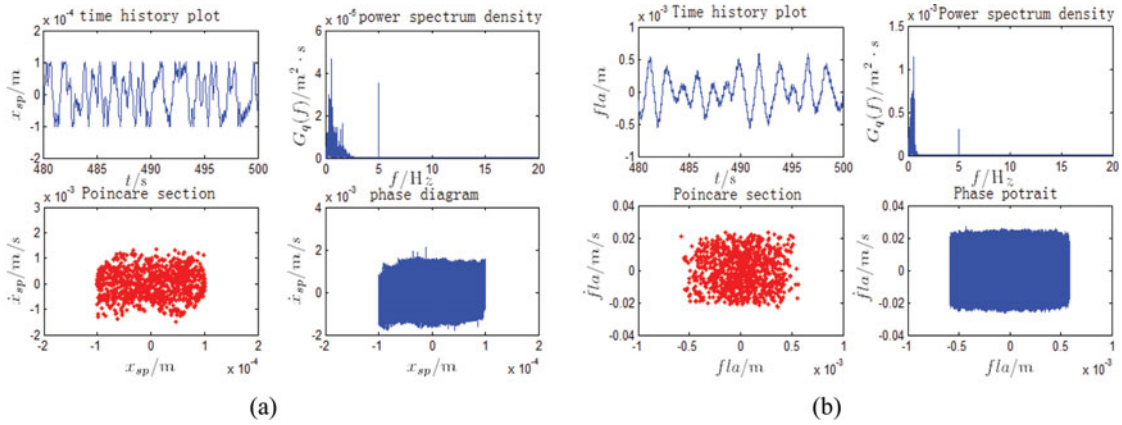

Fig. 15. Dynamic response of the system with flexible arm ($b = 100\ \mu$m, $\omega = 10\pi$).

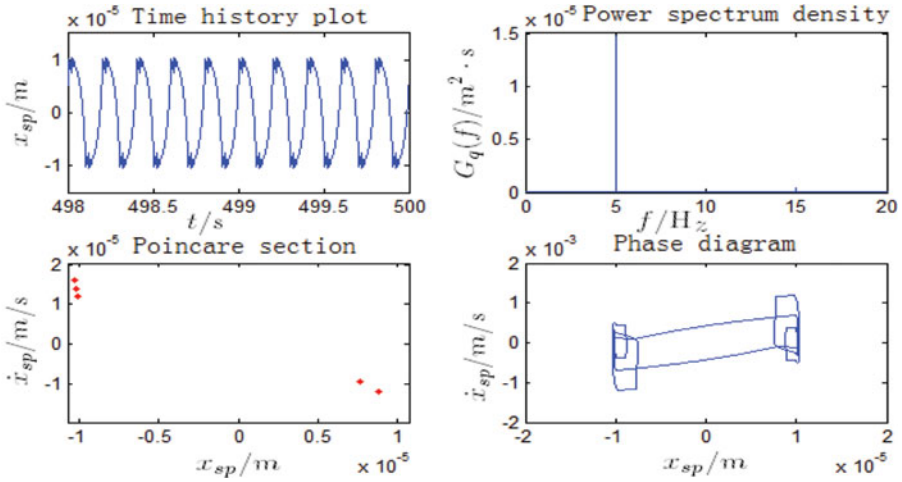

Fig. 16. Transmission error between the sun gear and planetary gear x_{sp} ($b = 10\ \mu$m, $\omega = 10\pi$).

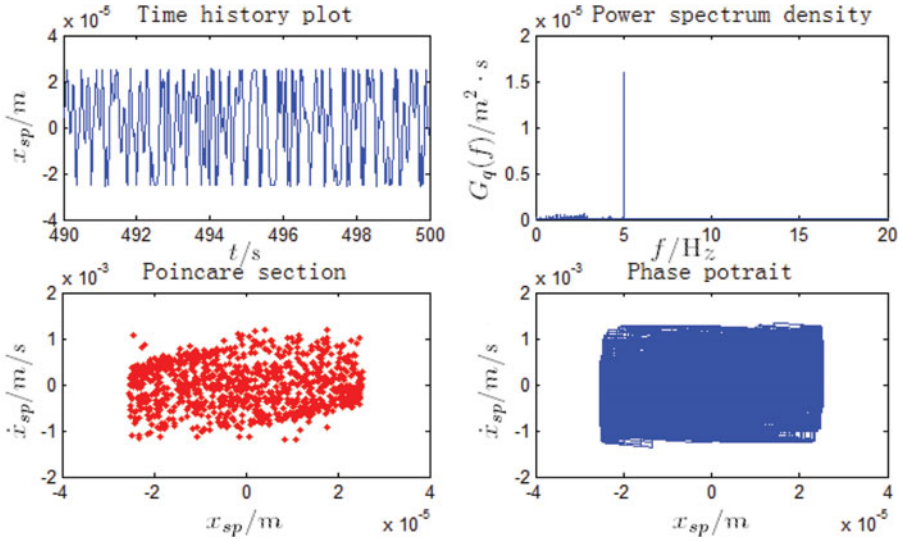

Fig. 17. Transmission error between the sun gear and planetary gear x_{sp} ($b = 25\ \mu$m, $\omega = 10\pi$).

https://doi.org/10.1017/S0263574714000915 Published online by Cambridge University Press

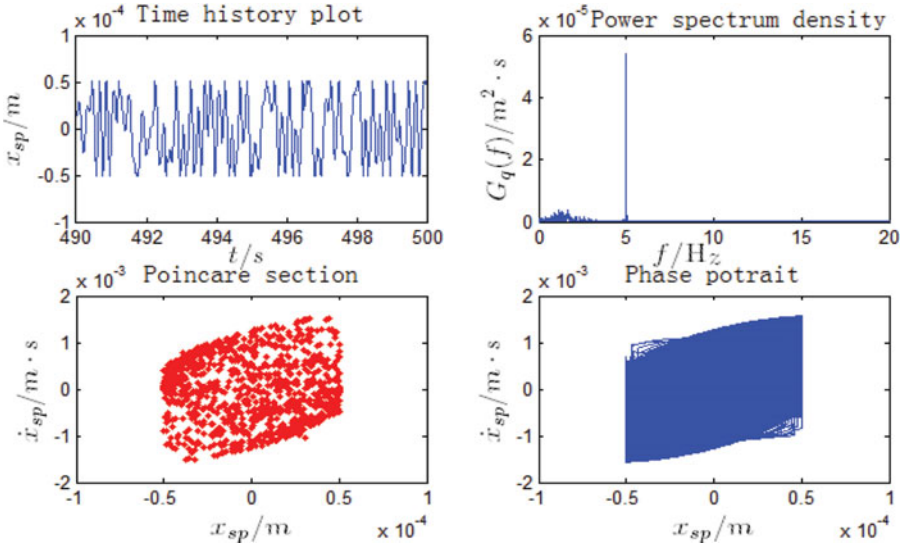

Fig. 18. Transmission error between the sun gear and planetary gear x_{sp} ($b = 50\ \mu$m, $\omega = 10\pi$).

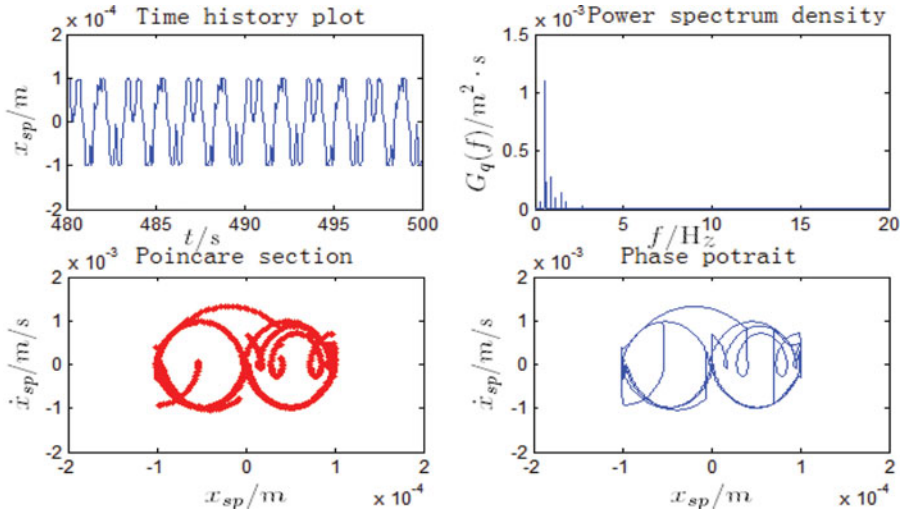

Fig. 19. Transmission error between the sun gear and planetary gear x_{sp} ($b = 100\ \mu$m, $\omega = 10\pi$).

(3) The positioning error at the end of the flexible manipulator arm is composed of two components: the transmission error due to the backlash of the gear reducer and the flexible deformation of the manipulator arm. The dominant component is the flexible deformation if the backlash is small, while the transmission error due to the backlash of the gear reducer gradually becomes the dominant component with increasing backlash.

(4) The flexible deformation amplitude of the manipulator arm is less affected by the backlash of the gear reducer, but the dominant mode of the manipulator arm is sensitive to the backlash which is the result of the nonlinearity of the gear reducer.

(5) The dynamic response of the flexible manipulator arm and that of the gear reducer are interactive. On the one hand, the dynamic response of the flexible manipulator arm is affected by that of the gear reducer, while on the other hand the coupling effect between them may lead to change in the dynamic behavior of the gear reducer.

https://doi.org/10.1017/S0263574714000915 Published online by Cambridge University Press

Acknowledgements
This research was supported by the Program for New Century Excellent Talents in University under grant NCET-10-0358, the provincial natural science research project of universities of Anhui, the National Natural Science Foundation of China under grant 50975071, and the Changzhou Research Program of Application Foundation under grant CJ20110006. These supports are gratefully acknowledged.

References

1. K. D. Santosha and E. Peter, "Dynamic analysis of flexible manipulators, a literature review," *Mech. Mach. Theory* **41**(7), 749–777 (2006).
2. W. Chen, "Dynamic modeling of multi-link flexible robotic manipulators," *Comput. Struct.* **79**(2), 183–195 (2001).
3. H. M. Yen, T. H. S. Li and Y. C. Chang, "Adaptive neural network based tracking control for electrically driven flexible-joint robots without velocity measurements," *Comput. Math. Appl.* **64**(5), 1022–1032 (2012).
4. C. Di Castri and A. Messina, "Exact modeling for control of flexible manipulators," *J. Vib. Control* **18**(10), 1526–1551 (2012).
5. E. Abedi, A. A. Nadooshan and S. Salehi, "Dynamic modeling of two flexible link manipulators," *World ACAD Sci. Eng.* **46**(3), 461–467 (2008).
6. F. Mehrdad and A. L. Stanislaw, "Dynamic modeling of spatial manipulators with flexible links and joints," *Comput. Struct.* **75**(4), 419–437 (2000).
7. B. O. Albedoor and A. A. Almusallam, "Dynamics of flexible-link and flexible-joint manipulator carrying a payload with rotary inertia," *Mech. Mach. Theory* **35**(6), 785–820 (2000).
8. B. Subudhi and A. S. Morris, "Dynamic modelling, simulation and control of a manipulator with flexible links and joints," *Robot. Auton. Syst.* **41**(4), 257–220 (2002).
9. A. Green and J. Z. Sasiadek, "Dynamics and trajectory tracking control of a two-link robot manipulator," *J. Vib. Control* **10**(10), 1415–1440 (2004).
10. R. Fotouhi, "Dynamic analysis of very flexible beams," *J. Sound Vib.* **35**(3), 521–533 (2007).
11. M. Vakil, R. Fotouhi and P. N. Nikiforuk, "A constrained Lagrange formulation of multilink planar flexible manipulator," *J. Vib. Acoust.* **130**(3), (2008). doi: 10.1115/1.2827455.
12. M. Kalyoncu, "Mathematical modelling and dynamic response of a multi-straight-line path tracing flexible robot manipulator with rotating-prismatic joint," *Appl. Math. Modelling* **32**(6), 1087–1098 (2008).
13. Z. L. Zhou, C. K. Mechefske and F. F. Xi, "Modeling of configuration-dependent flexible joints for a parallel robot," *Adv. Mech. Eng.* (2010). doi: 10.1155/2010/143961.
14. S. M. Yesiloglu and H. Temeltas, "Dynamical modeling of cooperating underactuated manipulators for space manipulation," *Adv. Robot.* **24**(3), 325–341 (2010).
15. M. Rognant, E. Couteile and P. Maurine. "A systematic procedure for the elastodynamic modeling and identification of robot manipulators," *IEEE Trans. Robot.* **26**(6), 1085–1093 (2010).
16. M. H. Korayem and H. R. Heidari, "Modeling and testing of moving base manipulators with elastic joints," *Latin Am. Appl. Res.* **41**(2), 157–163 (2011).
17. X. L. Chen, Y. Deng and S. S. Jia, "Rigid-flexible coupled dynamics modeling and analysis for a novel high-speed spatial parallel robot," *Adv. Sci. Lett.* **4**(8–10), 2595–2599 (2011).
18. P. Zarafshan and S. A. A. Moonsavian, "Rigid–flexible interactive dynamics modelling approach," *Math. Comput. Modelling Dyn. Syst.* **18**(2), 175–199 (2012).
19. M. Vakil, R. Fotouhi and P. N. Nikiforuk, "A new method for dynamic modeling of flexible-link flexible-joint manipulators," *J. Vib. Acoust.-Trans. ASME* **134**(1), (2012). doi: 10.1115/1.4004677.
20. B. Pratiher and S. Bhowmick, "Nonlinear dynamic analysis of a Cartesian manipulator carrying an end effector placed at an intermediate position," *Nonlinear Dyn.* **69**(1–2), 539–553 (2012).
21. Q. Y. Li, *Numerical Analysis* (Tsinghua University Press, Beijing, 2001).
22. T. Sun and Y. Shen, "Study on nonlinear dynamic behavior of planetary gear train dynamic model and governing equations," *Chin. J Mech. Eng.* 38(3): 6–10 (2002).